Available online at www.sciencedirect.com
ScienceDirect
Journal of Power Sources 161 (2006) 1012–1022
JOURNAL OF POWER SOURCES
www.elsevier.com/locate/jpowsour

Mathematical modeling of planar solid oxide fuel cells

M.M. Hussain [a], X. Li [a], I. Dincer [b,*]

[a] Department of Mechanical Engineering, University of Waterloo, Waterloo, Ontario, Canada N2L 3G1
[b] Faculty of Engineering and Applied Science, University of Ontario Institute of Technology, Oshawa, Ontario, Canada L1H 7K4

Received 14 April 2006; received in revised form 12 May 2006; accepted 16 May 2006
Available online 14 August 2006

Abstract

A mathematical model predicting the performance of planar solid oxide fuel cell (SOFC) has been developed. The model is fuel flexible, which implies not only pure H_2 but also any reformate composition (H_2, H_2O, CO, CO_2 and CH_4) can be used as a fuel. The important characteristic of this model is the consideration of reaction zone layers as finite volumes. Reaction zone layers are thin layers in the vicinity of the electrolyte where electrochemical reactions takes place to produce electrons, oxide ions and water vapor (and/or carbon dioxide). In addition, the effect of Knudsen diffusion is accounted in the porous electrode (backing) and reaction zone layers. The model can predict the performance of SOFC at various operating and design conditions. The predicted performance of SOFC is validated with the measured data found in the literature. An excellent agreement is obtained between the predicted performance and the experimental results. Moreover, the effect of various operating and design parameters on the performance of SOFC has been examined. It is found that the anode concentration overpotential in an anode-supported SOFC is about four orders of magnitude smaller than the anode ohmic overpotential even at higher current densities. Further, it is found that the single largest contributor to the total cell potential loss is ohmic overpotential and hence it needs to be minimized to enhance the cell performance.

Keywords: Solid oxide fuel cell (SOFC); Multi-component species; Reaction zone layers; Modeling

1. Introduction

Due to flexibility in fuel choice, solid oxide fuel cells (SOFCs) are receiving considerable attention for both small- and large-scale applications [1]. Not only pure H_2 but also any reformate composition consists of multi-component species such as H_2, H_2O, CO, CO_2 and CH_4 can be used as a fuel. Moreover, SOFCs can operate directly on hydrocarbon fuels with or without internal reforming, thereby reducing the cost of an external reformer [2]. Hence, fuel flexibility is one of the greatest advantages of SOFCs as compared to other types of fuel cells.

The planar-type design of SOFC has the potential to offer higher power density than the tubular design [3]. Due to its compactness, it can be stacked in resemblance to polymer electrolyte membrane (PEM) fuel cells to satisfy the power requirement of an application [4]. Higher power density of planar SOFC is due to the shorter current paths resulting in low ohmic overpotential. Moreover, planar SOFC is simple to fabricate and can be manufactured into various configurations [5]. However, the problems associated with the development and commercialization of planar SOFCs are requirement of high temperature gas seals, internal stresses in cell components due to non-uniform temperature distributions and high manufacturing cost.

In order to overcome the problems associated with planar SOFCs, much of the recent efforts are devoted to develop new materials and configurations to improve the performance at reduced operating temperatures [2,6–9]. By lowering the operating temperature of SOFC to around 700 °C, many of the problems associated with planar SOFC can be resolved. For instance, conventional stainless steel can be used for interconnectors instead of more expensive high chrome alloys or oxides and hence results in minimizing the material and manufacturing costs [10,11]. However, the ionic conductivity of the electrolyte decreases with the reduction of operating temperature. The reduction in ionic conductivity of the electrolyte resulting in higher ohmic overpotential at reduced operating temperatures can be minimized by either using electrode (anode or cathode) supported configuration of SOFC, wherein thin electrolytes of thicknesses in the range of 10–20 μm are deposited on the thick electrode (anode or cathode) or using composite ceramic elec-

* Corresponding author. Tel.: +1 905 721 8668/2573; fax: +1 905 721 3370.
E-mail address: Ibrahim.Dincer@uoit.ca (I. Dincer).

0378-7753/$ – see front matter © 2006 Elsevier B.V. All rights reserved.
doi:10.1016/j.jpowsour.2006.05.055

Nomenclature

A_v	reactive surface area per unit volume ($m^2\,m^{-3}$)
c_{H_2}	hydrogen concentration ($mol\,m^{-3}$)
$c_{H_2,ref}$	reference hydrogen concentration ($mol\,m^{-3}$)
c_{O_2}	oxygen concentration ($mol\,m^{-3}$)
$c_{O_2,ref}$	reference oxygen concentration ($mol\,m^{-3}$)
D_{ij}	binary diffusion coefficient ($m^2\,s^{-1}$)
$D_{Kn,i}$	Knudsen diffusion coefficient ($m^2\,s^{-1}$)
D_{ij}^{eff}	effective diffusion coefficient ($m^2\,s^{-1}$)
F	Faraday's constant ($96{,}487\,C\,mol^{-1}$)
J	current density ($A\,m^{-2}$)
J_e	electronic current density ($A\,m^{-2}$)
J_i	ionic current density ($A\,m^{-2}$)
$J_{0,ref}^{H_2}$	reference exchange current density for H_2 oxidation ($A\,m^{-2}$)
$J_{0,ref}^{O_2}$	reference exchange current density for O_2 reduction ($A\,m^{-2}$)
k_{bs}	backward reaction rate constant for shift reaction ($mol\,m^{-3}\,Pa^{-2}\,s^{-1}$)
k_{fs}	forward reaction rate constant for shift reaction ($mol\,m^{-3}\,Pa^{-2}\,s^{-1}$)
K_{ps}	equilibrium constant for shift reaction
M_i	molecular weight of species i ($kg\,mol^{-1}$)
n	moles of electrons transferred per mole reactant
n_{el}	number fraction of electron conducting particles in the reaction zone layers
n_{io}	number fraction of ion conducting particles in the reaction zone layers
n_t	total number of particles in the reaction zone layers per unit volume (m^{-3})
N_i	diffusive flux of species i ($mol\,m^{-2}\,s^{-1}$)
p	pressure (Pa)
p_{el}	probability of percolation of electron conducting particles in reaction zone layers
p_{io}	probability of percolation of ion conducting particles in reaction zone layers
r_{el}	radius of electron conducting particles in the reaction zone layers (m)
r_{io}	radius of ion conducting particles in the reaction zone layers (m)
r_s	volumetric shift reaction rate ($kg\,m^{-3}\,s^{-1}$)
R	universal gas constant ($8.3143\,J\,mol^{-1}\,K^{-1}$)
$\mathcal{R}_a$	volumetric current density produced due to H_2 oxidation ($A\,m^{-3}$)
$\mathcal{R}_c$	volumetric current density produced due to O_2 reduction ($A\,m^{-3}$)
$\dot{S}_{s,i}$	rate of production or consumption of species i ($kg\,m^{-3}\,s^{-1}$)
t_a	anode electrode (backing) thickness (m)
t_{arz}	anode reaction zone thickness (m)
t_c	cathode electrode (backing) thickness (m)
t_{crz}	cathode reaction zone thickness (m)
t_e	electrolyte thickness (m)
T	temperature (K)
T_{op}	operating temperature (K)
V_i	diffusion velocity of species i ($m\,s^{-1}$)
x	rectangular coordinate (m)
x_i	mole fraction of species i
Z	average coordination number
Z_{el}	coordination number of electron conducting particles in the reaction zone layers
Z_{io}	coordination number of ion conducting particles in the reaction zone layers

Greek symbols

α	charge transfer coefficient
γ_{H_2}	reaction order for H_2 oxidation
γ_{O_2}	reaction order for O_2 reduction
ε	porosity
η	overpotential (V)
κ	ionic conductivity ($S\,m^{-1}$)
ρ_i	partial density of species i ($kg\,m^{-3}$)
σ	electronic conductivity ($S\,m^{-1}$)
τ	tortuosity
ϕ_e	electronic potential (V)
ϕ_i	ionic potential (V)
Φ	volume fraction of electron conducting particles in the reaction zone layers

Subscripts

a	anode activation
bl	electrode (backing) layer
c	cathode activation
rl	reaction zone layer

Superscripts

eff	effective
e^-	electron conducting particles
O^{2-}	ion conducting particles

trolyte in an electrolyte supported configuration having high ionic conductivity at reduced temperatures [2].

Mathematical modeling is an essential aspect of SOFC technology development process. A numerical model facilitates research and development by minimizing the need of repetitive and costly experimentation. Numerical simulation of SOFCs provides a thorough understanding of how cell performance is affected by various operating and design parameters such as temperature, pressure, fuel composition, reactive surface area, pore size, porosity, tortuosity, thickness of various components, and ionic and electronic conductivities of ion-conducting and electronic-conducting particles of the electrode, respectively, and thus helps in optimizing cell and stack design.

Numerous models of SOFCs exists in the literature [3–5,7,12–14], varying in the number of assumptions employed. The common assumption in the existing SOFC models is the consideration of reaction zone layers as mathematical surfaces, treating them as boundary conditions. However, for composite electrodes such as those in SOFCs, the reaction zone layers

are spreaded out into the electrode some distance (10–50 μm) from the electrolyte/electrode interfaces [15–17]. Reaction zone layers are relatively thin layers where fuel and oxidant are electrochemically converted into electrical work, heat and water vapor (and/or carbon dioxide). Although Kim et al. [7] and Zhu and Kee [14] discussed about reaction zone layers but no one attempted to model these regions as finite volumes, rather treated them as boundary conditions.

Of the models existed in the literature, only Kim et al. [7] and Zhu and Kee [14] validated their models with the measured data available in the literature. The model of Kim et al. [7] is an empirical model with five fitting parameters and caters only binary mixtures in the electrodes. In addition, none of the existing complete cell models on SOFC incorporate micro characteristics of electrodes. Incorporation of micro parameters into the mathematical cell model not only helps in improving the accuracy of the model but also helps in quantitative design and optimization process [18].

The objective of the present study is to develop a mathematical model of SOFC satisfying the following requirements: (i) flexibility in fuel choice, not only pure H_2 but also any reformate composition (H_2, H_2O, CO, CO_2 and CH_4) can be used as a fuel, (ii) finite reaction zone layers, and (iii) incorporation of the micro characteristics of the electrodes. Moreover, the other objectives are to validate the developed model with the measured performance data available in the literature and to examine the effect of various operating and design parameters on the performance of SOFC.

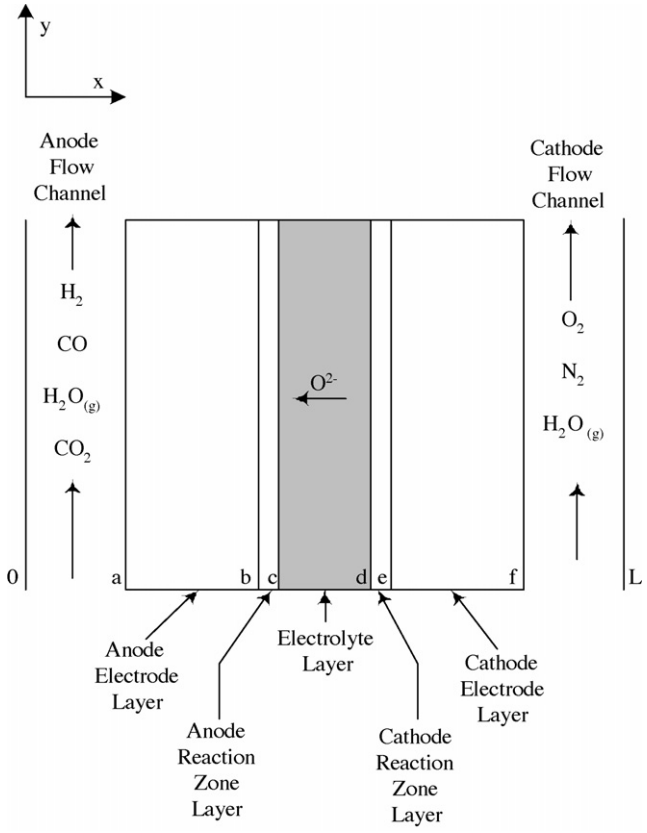

Fig. 1. Illustration of different layers of solid oxide fuel cell.

2. Model formulation

Fig. 1 illustrates different layers of SOFC. A typical SOFC consists of three major layers such as anode electrode layer, electrolyte layer and cathode electrode layer. Two additional layers, which are shown in Fig. 1 between the anode electrode layer and electrolyte layer and cathode electrode layer and electrolyte layer are called anode reaction zone layer and cathode reaction zone layer, respectively. The reaction zones on either side of the electrolyte are considered to be distinct layers because of the fact that the electrochemical reaction not only occurs on the interface between the anode and electrolyte, and the cathode and electrolyte but also extends to a depth of 10–50 μm inside electrode layers [15–17].

The cell is assumed to operate under steady state condition and the parameters vary in the x-direction only, as shown in Fig. 1. The temperature and total pressure are assumed to be uniform in the electrode and reaction zone layers. The convective flux is assumed to be negligible in the porous electrode and reaction zone layers when compared to the diffusive flux of gaseous species, which implies that the primary means of species transport in the porous electrode and reaction zone layers is diffusion [7]. The reactant gas mixtures are approximated as ideal gases with negligible viscous, Soret, Dofour and gravity effects. Since the reaction zone layers are considered as separate regions, there are no electrochemical reactions (either oxidation or reduction) in the electrode layers. The reaction zone layers consists of mixture of electron-conducting particles, electrolyte-conducting particles and void space occupied by gaseous species. Moreover, in the present study, it is assumed that there is no electrochemical oxidation of CO in the anode reaction zone layer. The electrolyte layer is assumed to be a dense solid with no interconnected porosity. With these assumptions the cell model is formulated and is described in the following sections.

2.1. Electrode (backing) layers

The processes that need to be modeled in the electrode layers are transport of multi-component species to and from the reaction sites in the reaction zone layers and electron migration through the solid portion of the porous structure. In Fig. 1, the electrode layers correspond to regions a–b and e–f.

The mathematical model for the processes occurring in the electrode layers are formulated by applying the conservation of species and conservation of electronic charge. The governing equations are described as follows:

$$\text{species}: \quad \nabla \cdot (\rho_i \vec{V}_i) = \dot{S}_{s,i} \tag{1}$$

$$\text{electronic charge}: \quad \nabla \cdot \vec{J}_e = 0 \tag{2}$$

where ρ_i is the partial density of species i, $\vec{V}_i$ is the species diffusion velocity, $\dot{S}_{s,i}$ is the species source term, and $\vec{J}_e$ is the electronic current density.

The diffusion velocity or in other words, the diffusion flux in the SOFC electrode layers can be determined using the modified Stefan-Maxwell equations incorporating Knudsen diffusion for

multi-component systems involving n species [19]:

$$-c\,\nabla x_i = \sum_{j=1,i}^{n} \frac{1}{D_{ij}^{\text{eff}}}(x_j\vec{N}_i - x_i\vec{N}_j) \tag{3}$$

where c is the concentration of the mixture, x_i the mole fraction of species i, $\vec{N}_i$ the diffusion flux of species i, and D_{ij}^{eff} the effective diffusion coefficient, defined as:

$$D_{ij}^{\text{eff}} = \frac{\varepsilon}{\tau}\left(\frac{D_{ij}D_{\text{Kn},i}}{D_{ij}+D_{\text{Kn},i}}\right) \tag{4}$$

where D_{ij} is ordinary or binary diffusion coefficient and $D_{\text{Kn},i}$ is Knudsen diffusion coefficient of species i, ε and τ are porosity and tortuosity of the electrode layers, respectively.

The species source term on the right-hand side of Eq. (1) represents the rate of production or consumption of species due to chemical reactions. Since there is no chemical reaction in the cathode electrode layer, the species source term in Eq. (1) vanishes, whereas in the anode electrode layer, it represents the volumetric production or consumption of species due to water-gas shift reaction given as:

$$\text{CO} + \text{H}_2\text{O} \rightleftharpoons \text{H}_2 + \text{CO}_2 \tag{5}$$

The volumetric reaction rate for the shift reaction can be written as:

$$r_{\text{s}} = k_{\text{fs}}c_{\text{CO}}c_{\text{H}_2\text{O}} - k_{\text{bs}}c_{\text{CO}_2}c_{\text{H}_2} \tag{6}$$

where k_{fs} and k_{bs} are forward and backward reaction rate constants for the water-gas shift reaction.

In terms of mole fraction, the volumetric reaction rate for shift reaction becomes:

$$r_{\text{s}} = \left(\frac{p}{RT}\right)^2[k_{\text{fs}}x_{\text{CO}}x_{\text{H}_2\text{O}} - k_{\text{bs}}x_{\text{CO}_2}x_{\text{H}_2}] \tag{7}$$

where p is the total pressure, R is the universal gas constant and T is the temperature.

The mass rates of production or consumption of various species in the anode electrode layer can be formulated as follows:

$$\dot{S}_{\text{s},\text{H}_2} = M_{\text{H}_2}r_{\text{s}} \tag{8}$$

$$\dot{S}_{\text{s},\text{H}_2\text{O}} = -M_{\text{H}_2\text{O}}r_{\text{s}} \tag{9}$$

$$\dot{S}_{\text{s,CO}} = -M_{\text{CO}}r_{\text{s}} \tag{10}$$

$$\dot{S}_{\text{s},\text{CO}_2} = M_{\text{CO}_2}r_{\text{s}} \tag{11}$$

where M_{H_2}, $M_{\text{H}_2\text{O}}$, M_{CO}, and M_{CO_2} are the molecular weights of H_2, H_2O, CO, and CO_2, respectively.

Using Ohm's law, the electronic current density given in Eq. (2) can be written in terms of electronic potential in the electrode layers as:

$$\text{electronic charge}: \quad \nabla\cdot(\sigma_{\text{bl}}^{\text{eff}}\nabla\phi_{\text{e}}) = 0 \tag{12}$$

where $\sigma_{\text{bl}}^{\text{eff}}$ is the effective electronic conductivity of the electrode layers, defined as:

$$\sigma_{\text{bl}}^{\text{eff}} = \left(\frac{1-\varepsilon}{\tau}\right)\sigma \tag{13}$$

where σ is the electronic conductivity of pure electrode layer materials.

2.2. Reaction zone layers

As mentioned in the previous sections, reaction zone layers are relatively thin layers where fuel and oxidant are electrochemically converted into electrical work, heat and water vapor. Often, these layers are idealized as mathematical surfaces, where the electrochemical reactions (oxidation or reduction) are assumed to occur at the localized triple phase boundary (TPB) between the electron-conducting particle, the ion-conducting particle and the reactant gas atmosphere. However, consideration of reaction zone layers as finite volumes would increase the number of reactive sites and leads to better agreement between the model prediction and the experimental observation [20]. Therefore, in this study the reaction zone layers are considered as finite volumes rather than mathematical surfaces, comprising of electron-conducting particles, ion-conducting particles and void spaces occupied by the gases. The processes which need to be modeled in these layers are transport of gaseous species with chemical and electrochemical reactions and electron and ion migration in the electron- and ion-conducting particles, respectively.

The conservation of species equation governing the transport of multi-component species in the reaction zone layers is similar to the electrode layers given in Eq. (1) except the source term, which also accounts for species consumption or production due to electrochemical reactions. Again, the modified Stefan-Maxwell equation given in Eq. (3) is used to model diffusion flux in the reaction zone layers. The equations governing the migration of electrons and ions in the electron- and ion-conducting particles of the reaction zone layers are described as follows:

- anode reaction zone layer:

$$\text{electronic charge}: \quad \nabla\cdot\vec{J}_{\text{e}} = \mathcal{R}_{\text{a}} \tag{14}$$

$$\text{ionic charge}: \quad \nabla\cdot\vec{J}_{\text{i}} = -\mathcal{R}_{\text{a}} \tag{15}$$

- cathode reaction zone layer:

$$\text{electronic charge}: \quad \nabla\cdot\vec{J}_{\text{e}} = -\mathcal{R}_{\text{c}} \tag{16}$$

$$\text{ionic charge}: \quad \nabla\cdot\vec{J}_{\text{i}} = \mathcal{R}_{\text{c}} \tag{17}$$

where $\mathcal{R}_{\text{a}}$ and $\mathcal{R}_{\text{c}}$ are volumetric current densities produced in the anode and cathode reaction zone layers due to H_2 oxidation and O_2 reduction reactions, respectively, which are given by the general Butler-Volmer equations as:

$$\mathcal{R}_{\text{a}} = A_{\text{v}}J_{0,\text{ref}}^{\text{H}_2}\left(\frac{c_{\text{H}_2}}{c_{\text{H}_2,\text{ref}}}\right)^{\gamma_{\text{H}_2}} \times\left\{\exp\left(\frac{\alpha n F\eta_{\text{a}}}{RT}\right) - \exp\left(-\frac{(1-\alpha)nF\eta_{\text{a}}}{RT}\right)\right\} \tag{18}$$

$$\mathcal{R}_c = A_v J_{0,ref}^{O_2} \left(\frac{c_{O_2}}{c_{O_2,ref}} \right)^{\gamma_{O_2}} \times \left\{ \exp\left(\frac{\alpha n F \eta_c}{RT} \right) - \exp\left(-\frac{(1-\alpha) n F \eta_c}{RT} \right) \right\} \quad (19)$$

where A_v is the actual reactive surface area per unit volume, $J_{0,ref}^{H_2}$ and $J_{0,ref}^{O_2}$ are reference exchange current densities for H_2 oxidation and O_2 reduction at the reference concentrations $c_{H_2,ref}$ and $c_{O_2,ref}$, respectively, α the charge transfer coefficient (or symmetry factor), whose value lies between 0 and 1, n the number of electrons participating in the electrochemical reaction and η_a and η_c are anode and cathode activation overpotentials, respectively, defined as:

$$\eta_a = \phi_i - \phi_e \quad (20)$$

$$\eta_c = \phi_e - \phi_i \quad (21)$$

The expression used to model reactive surface area per unit volume (A_v) was developed by Costamagna et al. [21] based on the particle coordination number in binary random packing of spheres, given as:

$$A_v = \pi \sin^2\theta r_{el}^2 n_t n_{el} n_{io} \frac{Z_{el} Z_{io}}{Z} p_{el} p_{io} \quad (22)$$

where θ is the contact angle between electron and ion conducting particles in the reaction zone layer, r_{el} is the radius of the electron conducting particles, n_t is the total number of particles per unit volume, n_{el} and n_{io} are the number fraction of electron and ion conducting particles in the reaction zone layers, respectively, Z_{el} and Z_{io} are the coordination numbers of electron and ion conducting particles in the reaction zone layers, respectively, Z is the total average number of contacts of each particle and p_{el} and p_{io} are the probabilities of electron and ion conducting particles in the reaction zone layers, respectively.

The parameters required to obtain reactive surface area per unit volume (A_v) can be calculated from [18,21]:

$$n_t = \frac{1-\varepsilon}{(4/3)\pi r_{el}^3 [n_{el} + (1-n_{el})(r_{io}/r_{el})^3]} \quad (23)$$

where ε is the porosity of the reaction zone layers, and:

$$n_{el} = \frac{\Phi}{\left[\Phi + \left((1-\Phi)/(r_{io}/r_{el})^3\right)\right]} \quad (24)$$

where Φ is the volume fraction of the electron conducting particles in the reaction zone layers.

$$Z_{el} = 3 + \frac{Z-3}{[n_{el} + (1-n_{el})(r_{io}/r_{el})^2]} \quad (25)$$

$$Z_{io} = 3 + \frac{(Z-3)(r_{io}/r_{el})^2}{[n_{el} + (1-n_{el})(r_{io}/r_{el})^2]} \quad (26)$$

where Z is the total average coordination number, equal to 6 [18].

$$p_{el} = \left[1 - \left(2 - \frac{Z_{el-el}}{2} \right)^{2.5} \right]^{0.4} \quad (27)$$

$$p_{io} = \left[1 - \left(2 - \frac{Z_{io-io}}{2} \right)^{2.5} \right]^{0.4} \quad (28)$$

where

$$Z_{el-el} = \frac{n_{el} Z_{el}^2}{Z} \quad (29)$$

$$Z_{io-io} = \frac{n_{io} Z_{io}^2}{Z} \quad (30)$$

The species source terms in the anode and cathode reaction zone layers due to electrochemical reactions are related to volumetric current density through Faraday's law of electrochemical reaction and are described as follows:

- anode reaction zone layer:

$$\dot{S}_{s,i} = -\frac{\nu_i M_i \mathcal{R}_a}{nF} \quad (31)$$

where M_i is the molecular weight of the species i, $\mathcal{R}_a$ is the volumetric current density produced due to H_2 oxidation reaction given in Eq. (18), n is the number of electrons participating in the electrochemical reaction, F is the Faraday's constant, and ν_i is the stoichiometric coefficient of the species involved in the oxidation reaction expressed in the following form [22]:

$$H_2 + O^{2-} - H_2O \rightarrow 2e^- \quad (32)$$

- cathode reaction zone layer:

$$\dot{S}_{s,i} = -\frac{\nu_i M_i \mathcal{R}_c}{nF} \quad (33)$$

where $\mathcal{R}_c$ is the volumetric current density produced due to O_2 reduction reaction given in Eq. (19), expressed in the following form [22]:

$$\frac{1}{2}O_2 - O^{2-} \rightarrow 2e^- \quad (34)$$

Converting the electronic and ionic current densities given in Eqs. (14)–(17) into electronic and ionic potentials through Ohm's law, Eqs. (14)–(17) becomes:

- anode reaction zone layer:

$$\text{electronic charge}: \quad \nabla \cdot (\sigma_{rl}^{eff} \nabla \phi_e) = -\mathcal{R}_a \quad (35)$$

$$\text{ionic charge}: \quad \nabla \cdot (\sigma_{bl}^{eff} \nabla \phi_i) = \mathcal{R}_a \quad (36)$$

- cathode reaction zone layer:

$$\text{electronic charge}: \quad \nabla \cdot (\sigma_{rl}^{eff} \nabla \phi_e) = \mathcal{R}_c \quad (37)$$

$$\text{ionic charge}: \quad \nabla \cdot (\sigma_{rl}^{eff} \nabla \phi_i) = -\mathcal{R}_c \quad (38)$$

where the effective electronic and ionic conductivities in the reaction zone layers are defined as [23]:

$$\sigma_{rl}^{eff} = \Phi \left(\frac{1-\varepsilon}{\tau} \right) \sigma \quad (39)$$

$$\kappa_{\mathrm{rl}}^{\mathrm{eff}} = (1-\Phi)\left(\frac{1-\varepsilon}{\tau}\right)\kappa \tag{40}$$

where Φ is the volume fraction of the electron conducting particles in the reaction zone layer, σ and κ are the conductivities of pure electron and ion-conducting materials, respectively.

2.3. Electrolyte layer

Electrolyte layer in SOFC is fully dense with no interconnected porosity. The major function of the electrolyte is to conduct oxide ions produced in the cathode reaction zone layer to the anode reaction zone layer, thus completing the electrical circuit. The conservation equation governing the migration of oxide ion in the electrolyte layer is given as:

$$\nabla \cdot \vec{J}_{\mathrm{i}} = 0 \tag{41}$$

where J_{i} is the ionic current density, which is equal to the total current density J.

Using Ohm's law, the ionic current density can be expressed in terms of ionic potential and the above conservation equation becomes:

$$\nabla \cdot (\kappa \nabla \phi_{\mathrm{i}}) = 0 \tag{42}$$

where κ is the ionic conductivity of the electrolyte.

The governing equations used in the model formulation of different components of SOFC are summarized in Table 1.

2.4. Boundary conditions

The location at which boundary conditions are needed to complete the mathematical formulation are illustrated in Fig. 1 as "a", "b", "c", "d", "e" and "f". Locations "a" and "f" are the interfaces between the fuel channel and anode electrode (backing) layer and air channel and cathode electrode (backing) layer, respectively; the boundary conditions at these location are specified boundary conditions, where the composition of gaseous species and electronic potential are specified. The boundary conditions at the interfaces between the anode electrode and anode reaction zone layers (location "b") and the cathode electrode and cathode reaction zone layers (location "e") are continuous flux boundary conditions for gaseous species and electronic potential, where the diffusion flux and electronic current density are continuous, whereas insulated boundary condition for ionic potential, which implies ionic current density is zero. At locations "c" and "d", the interfaces between the anode reaction zone layer and electrolyte layer, and the cathode reaction zone layer and electrolyte layer, the diffusion flux and electronic current density are zero, whereas the ionic current density is continuous and is equal to the total current density. Mathematically, the boundary conditions at different locations in Fig. 1 can be expressed as:

$$\begin{aligned}
&\text{at } x = \text{"a" and "f"}: && x_i = \text{specified}, \quad \phi_{\mathrm{e}} = \text{specified};\\
&\text{at } x = \text{"b" and "e"}: && N_i|_{\mathrm{bl}} = N_i|_{\mathrm{rz}}, \quad J_{\mathrm{e}}|_{\mathrm{bl}} = J_{\mathrm{e}}|_{\mathrm{rl}}, \quad J_{\mathrm{i}} = 0;\\
&\text{at } x = \text{"c" and "d"}: && N_i = 0, \quad J_{\mathrm{e}} = 0, \quad J_{\mathrm{i}} = J.
\end{aligned}$$

3. Model validation

Since the mathematical model presented above is based on the conservation principle, the numerical method used to discretize the governing equations is a well-known method, often referred to as "finite-volume method" or "control-volume method". The discretized governing equations form a system of algebraic equations whose solution can be obtained using a direct method or an iterative method. For the present problem, an iterative method is used because of the fact that the coefficients of the discretized algebraic equations are not constants but are functions of the variables evaluated at grid points.

Using the parameters listed in Table 2, the predicted cell performance is compared with the experimental data found in the literature [24], and is shown in Fig. 2. The performance of the cell is predicted when the cell is supplied with 95% H_2 and 5% H_2O as fuel, operating at a temperature and pressure of 1073 K and 1 atm, respectively. Oxygen composition in the ambient air is used as oxidant. It can be seen that the present model predictions agree well with the experimental results. It is worth mentioning that all the parameters used in the model validation are obtained from Rogers et al. [24] except the parameters given with the references. The value of tortuosity is varied to obtain the

Table 1
Governing equations

Cell layers	Conservation of species	Conservation of electronic charge	Conservation of ionic charge
Anode electrode layer	$\nabla \cdot (\vec{N}_i M_i) = \dot{S}_{\mathrm{s},i}, \quad -\nabla x_i = \sum_{j=1,i}^{n} \frac{1}{D_{ij}^{\mathrm{eff}}}(x_j \vec{N}_i - x_i \vec{N}_j)$	$\nabla \cdot (\sigma_{\mathrm{bl}}^{\mathrm{eff}} \nabla \phi_{\mathrm{e}}) = 0$	–
Cathode electrode layer	$\nabla \cdot (\vec{N}_i M_i) = 0, \quad -\nabla x_i = \sum_{j=1,i}^{n} \frac{1}{D_{ij}^{\mathrm{eff}}}(x_j \vec{N}_i - x_i \vec{N}_j)$	$\nabla \cdot (\sigma_{\mathrm{bl}}^{\mathrm{eff}} \nabla \phi_{\mathrm{e}}) = 0$	–
Anode reaction zone layer	$\nabla \cdot (\vec{N}_i M_i) = \dot{S}_{\mathrm{s},i}, \quad -\nabla x_i = \sum_{j=1,i}^{n} \frac{1}{D_{ij}^{\mathrm{eff}}}(x_j \vec{N}_i - x_i \vec{N}_j)$	$\nabla \cdot (\sigma_{\mathrm{rl}}^{\mathrm{eff}} \nabla \phi_{\mathrm{e}}) = -\mathcal{R}_{\mathrm{a}}$	$\nabla \cdot (\sigma_{\mathrm{bl}}^{\mathrm{eff}} \nabla \phi_{\mathrm{i}}) = \mathcal{R}_{\mathrm{a}}$
Cathode reaction zone layer	$\nabla \cdot (\vec{N}_i M_i) = \dot{S}_{\mathrm{s},i}, \quad -\nabla x_i = \sum_{j=1,i}^{n} \frac{1}{D_{ij}^{\mathrm{eff}}}(x_j \vec{N}_i - x_i \vec{N}_j)$	$\nabla \cdot (\sigma_{\mathrm{rl}}^{\mathrm{eff}} \nabla \phi_{\mathrm{e}}) = \mathcal{R}_{\mathrm{c}}$	$\nabla \cdot (\sigma_{\mathrm{rl}}^{\mathrm{eff}} \nabla \phi_{\mathrm{i}}) = -\mathcal{R}_{\mathrm{c}}$
Electrolyte layer	–	–	$\nabla \cdot (\kappa \nabla \phi_{\mathrm{i}}) = 0$

Table 2
Parameters used for model validation

Operating temperature, T_{op} (K)	1073.0
Total pressure, p (atm)	1.0
Fuel composition, $x_{H_2}; x_{H_2O}$	0.95; 0.05
Air composition, $x_{O_2}; x_{N_2}$	0.21; 0.79
Anode conductivity, σ (S m^{-1})	71428.57
Cathode conductivity, σ (S m^{-1})	5376.34
Electrolyte conductivity, κ (S m^{-1})	0.64
Anode electrode layer thickness, t_a (μm)	1000.0
Cathode electrode layer thickness, t_c (μm)	50.0
Anode reaction zone layer thickness, t_{arz} (μm)	20.0
Cathode reaction zone layer thickness, t_{crz} (μm)	20.0
Electrolyte thickness, t_e (μm)	10.0
Porosity of anode and cathode, ε	0.375
Tortuosity of anode and cathode, τ	2.75 [20]
Pore diameter of anode and cathode, d_p (μm)	1.5 [7]
Contact angle between e^- and O^{2-} conducting particles, θ (°)	15 [21]
Radius of e^- conducting particles, r_{el} (μm)	0.1 [18,29]
Radius of O^{2-} conducting particles, r_{io} (μm)	0.1 [18,29]
Volume fraction of e^- conducting particles, Φ	0.5 [21,23]
Reference H_2 concentration, c_{H_2} (mol m^{-3})	10.78
Reference O_2 concentration, c_{O_2} (mol m^{-3})	2.38
Reference exchange current density for H_2 oxidation, $J^{H_2}_{0,ref}$ (A m^{-2})	1320 [7]
Reference exchange current density for O_2 reduction, $J^{O_2}_{0,ref}$ (A m^{-2})	400 [21]
Reaction order for H_2 oxidation, γ_{H_2}	0.5
Reaction order for O_2 reduction, γ_{O_2}	0.5

Source: Rogers et al. [24].

best agreement between the present model predictions and the experimental results shown in Fig. 2, since the value reported by Rogers et al. [24] is unity. The typical tortuosity value for SOFC electrodes is in the range of 2–6 [20,25]. Hence, the tortuosity value of 2.75 used in the present model predictions is in the typical range for SOFC electrodes and provides the best agreement with the experimental results. The R^2-value, an indicator between 0 and 1, reveals how closely the predicted values correspond to the experimental data, is obtained for the present model as 0.988.

4. Results and discussion

The developed SOFC model can be used to investigate the effect of operating and design parameters on the cell performance. The fuel composition used in the simulation is listed in Table 3. Oxygen composition in the ambient air is used as oxidant. The model base case parameters derived from the data available in the literature are given in Table 4. The most significant difference between the base case and model validation parameters given in Table 2 is the thickness of the anode electrode layer. Typical thickness of the anode electrode layer reported in the literature for an anode-supported SOFC is 2 mm [10,16,26]. Since SOFCs are fuel flexible, methane reformate fuel composition given in Table 3 is used in the present simulation. Further, water-gas shift reaction is considered in the anode electrode and reaction zone layers.

The cell performance resulting from the base case parameters is shown in Fig. 3. It can be seen that the most significant contribution to the cell potential loss is from the anode side of the cell. The anode overpotential includes the anode activation overpotential due to the resistance to the charge transfer reaction, anode ohmic overpotential due to the resistance to the flow of electrons and ions in the anode reaction zone layer and resistance to the flow of electrons in the anode electrode (backing) layer and anode concentration overpotential due to the resistance to

Table 3
Mole fraction of methane reformate used in the simulation

Mole fraction	Value
x_{H_2}	0.410
x_{H_2O}	0.435
x_{CO}	0.090
x_{CO_2}	0.065

Source: Rajesh et al. [31].

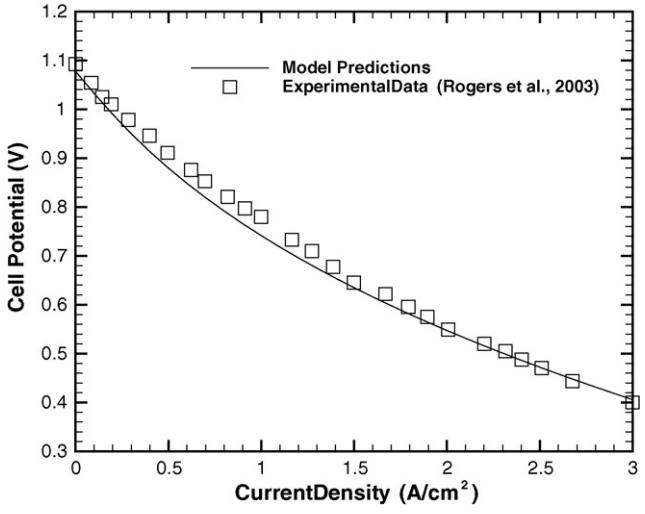

Fig. 2. Comparison between the model predictions and experimental results of Rogers et al. [24].

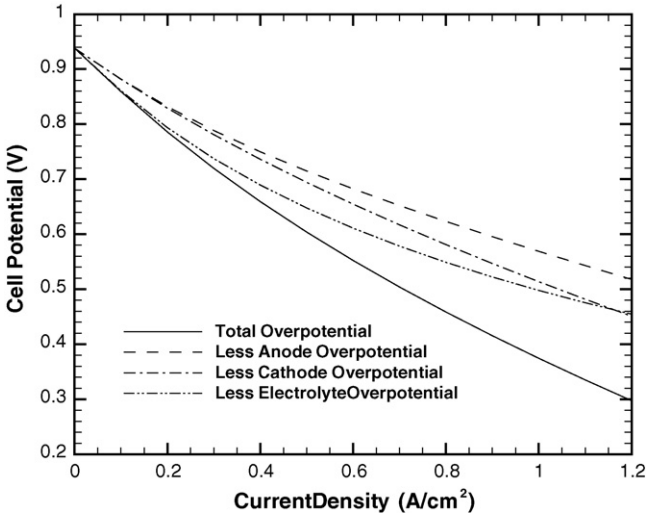

Fig. 3. Base case cell performance using the parameters in Table 4.

Table 4
Base case parameters used in the simulation

Operating temperature, T_{op} (K)	1073.0
Total pressure, p (atm)	1.0
Anode electrode layer thickness, t_a (μm)	2000.0
Cathode electrode layer thickness, t_c (μm)	50.0
Anode reaction zone layer thickness, t_{arz} (μm)	50.0
Cathode reaction zone layer thickness, t_{crz} (μm)	10.0
Electrolyte thickness, t_e (μm)	40.0
Anode conductivity, σ (S m^{-1})	$[((9.5 \times 10^7)/T) \exp(-1150/T)]$ [12]
Cathode conductivity, σ (S m^{-1})	$[((4.2 \times 10^7)/T) \exp(-1200/T)]$ [12]
Electrolyte conductivity, κ (S m^{-1})	$3.34 \times 10^4 \exp(-10300/T)$ [12]
Porosity of anode and cathode, ε	0.3 [18]
Tortuosity of anode and cathode, τ	4.5 [10]
Pore diameter of anode and cathode, d_p (μm)	1.0 [7]
Contact angle between e^- and O^{2-} conducting particles, θ (°)	15 [21]
Radius of e^- conducting particles, r_{el} (μm)	0.1 [18,29]
Radius of O^{2-} conducting particles, r_{io} (μm)	0.1 [18,29]
Volume fraction of e^- conducting particles, Φ	0.5 [21,23]
Reference H_2 concentration, c_{H_2} (mol m^{-3})	10.78
Reference O_2 concentration, c_{O_2} (mol m^{-3})	2.38
Reference exchange current density for H_2 oxidation, $J_{0,ref}^{H_2}$ (A m^{-2})	1320 [7]
Reference exchange current density for O_2 reduction, $J_{0,ref}^{O_2}$ (A m^{-2})	400 [21]
Reaction order for H_2 oxidation, γ_{H_2}	0.5
Reaction order for O_2 reduction, γ_{O_2}	0.5
Forward reaction rate constant for the shift reaction, k_{fs} (mol m^{-3} Pa^{-2} s^{-1})	$0.0171 \exp(-103191/RT)$
Backward reaction rate constant for the shift reaction, k_{bs}	k_{fs}/K_{ps}
	$K_{ps} = \exp(-0.2935\zeta^3 + 0.635\zeta^2 + 4.1788\zeta + 0.3169)$, $\zeta = (1000/T(\mathrm{K})) - 1$ [32]

the flow of reactant species through the void spaces. The cathode overpotential also includes all forms of overpotentials (activation, ohmic and concentration). The electrolyte overpotential is due to the resistance to the ion transport through the electrolyte layer. Although the thickness of the cathode (includes backing and reaction zone layer) and electrolyte are relatively thin in anode-supported SOFC but the potential loss in these components are significant and hence cannot be neglected.

The composition, morphology and thickness of the reaction zone layers has a significant impact on the cell performance and a substantial amount of research is being devoted in optimizing these layers [18,21,23,27–29]. The parameters which are of significant importance for enhancing cell performance are an efficient triple phase boundary (TPB) area or active area for electrochemical reaction, and high ionic and electronic conductivities in the ion and electron conducting particles [21]. According to Costamagna et al. [21], the largest active area is achieved when the dimensions and volume fractions of the ion conducting and electron conducting particles are equal. Therefore, in the base case cell performance shown in Fig. 3, the dimensions and volume fractions of the ion conducting and electron conducting particles are set to be equal.

Often, it is reported that the contribution of concentration overpotential in anode-supported SOFC is significant due to thick anode [7,10], but the cell performance obtained at the base case conditions reveals that the anode concentration overpotential is about four orders of magnitude smaller than the anode ohmic overpotential even at higher current densities. This can be evident from Fig. 4. Moreover, the contribution of anode activation overpotential is found to be negligible. On the other hand, due to the thin cathode, the contribution of cathode concentration overpotential to the total cell potential is negligible, whereas cathode activation overpotential is about two orders of magnitude smaller than cathode ohmic overpotential, as shown in Fig. 5. It is clear from Figs. 4 and 5 that the greatest contributor to the cell potential loss is ohmic overpotential. More specifically, it is the ionic conductivity of the ion conducting particles in the reaction zone layers, which is contributing to the overall ohmic overpotential, and hence it needs to be enhanced to improve the cell performance.

The effect of temperature on cell performance is shown in Fig. 6. The other operating and design parameters are in accordance with the base case parameters listed in Table 4. It can be seen that with the increase of temperature, the ideal or reversible cell potential (potential at zero current density) decreases, whereas the actual cell potential increases with the increase of temperature, in other words, cell performance increases with the increase of temperature. Increasing the temperature not only enhances the rate of electrochemical reaction at the reaction sites

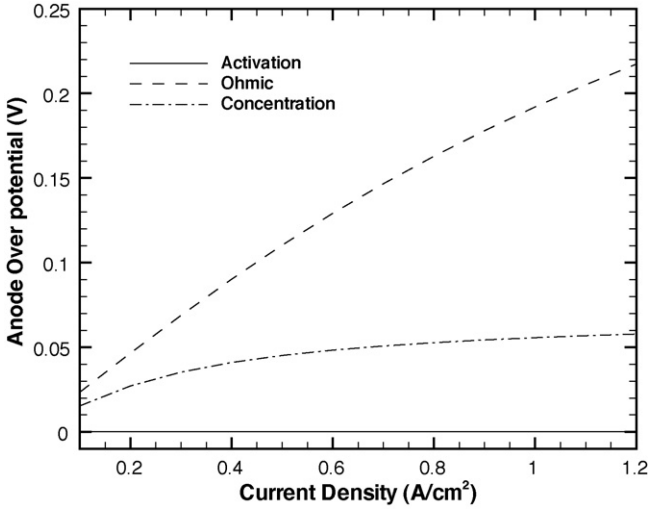

Fig. 4. Anode overpotentials at the base case conditions given in Table 4.

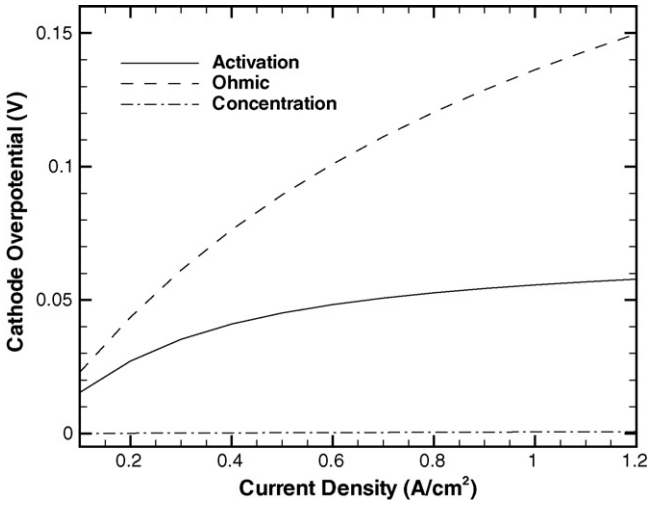

Fig. 5. Cathode overpotentials at base case conditions given in Table 4.

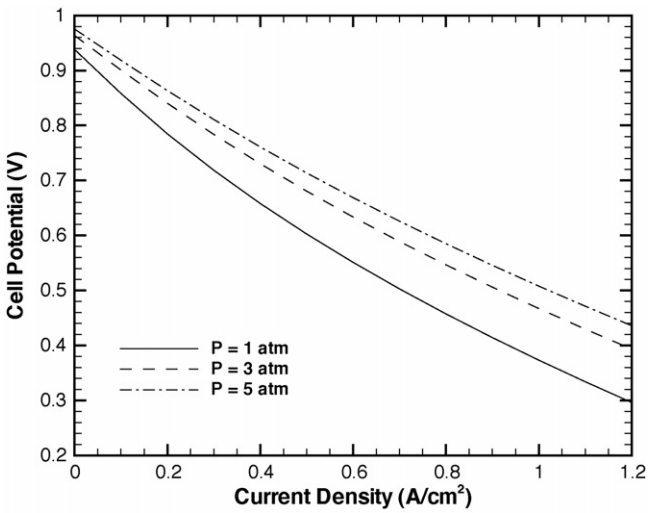

Fig. 7. Effect of pressure on cell performance.

but also increases the electronic and ionic conductivities of the electron and ion conducting particles, respectively, which in turn minimizes the ohmic contribution to the total cell potential loss and thereby enhances the cell performance.

Fig. 7 shows the effect of pressure on the performance of the cell. The temperature and other parameters are set as base case parameters listed in Table 4. It can be observed that increasing the pressure not only increases the reversible cell potential but also increases the actual cell potential. With the increase of pressure, the reactant concentration at the reaction sites increases, which in turn enhances the rate of electrochemical reaction and rate of mass transport resulting in the minimization of anode and cathode overpotentials and hence better performance. However, increase in pressure results in other problems such as limitation on material selection, gas sealing and mechanical strength of the cell components [30].

The effect of porosity on the performance of the cell is shown in Fig. 8. The temperature and pressure were set at 1073 K and 1 atm, and all other parameters are the same as that of base case parameters given in Table 4. It can be seen that increasing the porosity of the cell components decreases the cell performance. Increasing the porosity increases the void fraction and decreases the solid fraction of the porous layers resulting in the reduction of the active surface area available for the electrochemical reaction. Moreover, the effective ionic and electron conductivities of the porous layers decreases with the increase of porosity, which results in the increase of ohmic overpotential. Although the concentration overpotential decreases with the increase of porosity due to the increased mass transport rates but the cell performance decreases due to increased ohmic overpotential with porosity.

Fig. 9 depicts the effect of tortuosity on cell performance. The temperature and pressure were again set at 1073 K and 1 atm. It can be observed that increasing the tortuosity of the porous layers decreases the performance of the cell. Increasing the tortuosity of the porous layers means increasing the tortuous path, which adds additional resistance to the reactant species diffusing through the porous layers resulting in the reduction of reactant concentration at the reaction sites and thereby decreasing the rate

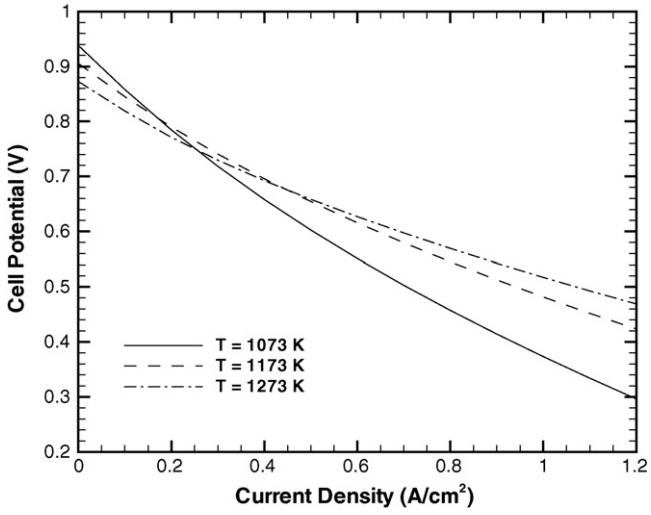

Fig. 6. Effect of temperature on cell performance.

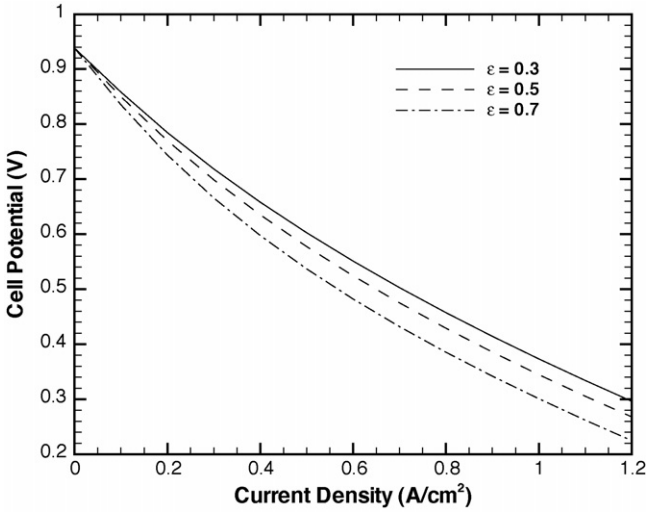

Fig. 8. Effect of porosity on cell performance.

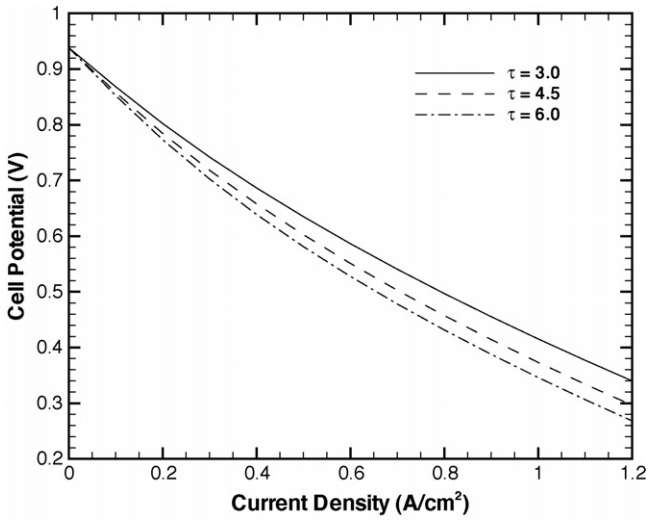

Fig. 9. Effect of tortuosity on cell performance.

of electrochemical reaction. In addition, the effective ionic and electronic conductivities decreases with the increase of tortuosity resulting in the increase of ohmic overpotential and hence cell performance decreases with the increase of tortuosity.

The effect of volume fraction of electron conducting particles of reaction zone layers on cell performance is shown in Fig. 10. Again the operating and other design parameters are kept similar to that of base parameters listed in Table 4. It can be seen that cell performance increases when the volume fraction of electron conducting particles (Φ) in the reaction zone layers is increased from 0.4 to 0.5, and it decreases when Φ is increased from 0.5 to 0.6. The increase and decrease in cell performance with volume fraction of electron conducting particles demonstrate the fact that the largest active area is achieved when the dimensions and volume fractions of the ion conducting and electron conducting particles are equal [21]. When Φ equals to 0.5, the volume fraction of ion conducting particles $(1 - \Phi)$ becomes equal to the volume fraction of electron conducting particles resulting in the largest active area for electrochemical reaction and hence the best performance. Moreover, the effective ionic and electronic conductivities in the reaction zone layers are functions of the volume fraction of electron conducting particles, increasing Φ beyond 0.5 increases the effective electronic conductivity but decreases the effective ionic conductivity, which results in increasing the ohmic overpotential and thereby decreasing the cell performance.

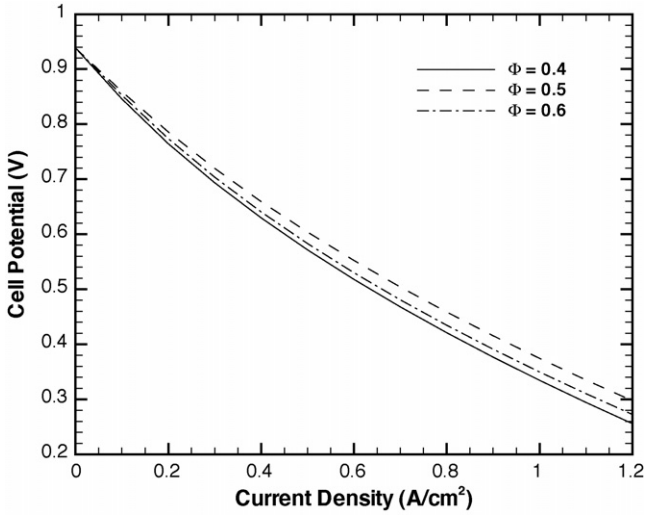

Fig. 10. Effect of volume fraction of electron conducting particles on cell performance.

5. Conclusions

A mathematical model of solid oxide fuel cell (SOFC) has been developed, which can predict the performance at various operating and design conditions. The model is fuel flexible, which can predict the performance for not only pure H_2 but also any reformate composition as fuel. The important feature of this model is the consideration of reaction zone layers as finite volumes, which were often treated as mathematical surfaces (boundary conditions) in the existing models. In addition, micro characteristics of the electrodes are incorporated into the model. The predicted performance is validated with the experimental data found in the literature. An excellent agreement is obtained between the predicted values and the measured data with R^2-value as high as 0.988. Moreover, the effect of operating and design conditions on the cell performance has been examined. It is found that the most significant contribution to the cell potential loss is from the anode side of the cell in an anode-supported SOFC, and anode concentration overpotential at base case conditions is about four orders of magnitude smaller than the anode ohmic overpotential even at higher current densities. Overall, ohmic overpotential is the single largest contributor to the total cell potential loss and hence needs to be minimized to enhance the cell performance.

Acknowledgements

The financial support of Auto21 Network of Centres of Excellence of Canada, and the Natural Sciences and Engineering Research Council of Canada is greatly acknowledged.

References

[1] R.J. Gorte, Recent developments towards commercialization of solid oxide fuel cells, AIChE J. 51 (2005) 2377–2381.
[2] J. Yuan, B. Sunden, Analysis of intermediate temperature solid oxide fuel cell transport processes and performance, Trans. ASME J. Heat Transfer 127 (2005) 1380–1390.
[3] M.A. Khaleel, Z. Lin, P. Singh, W. Surdoval, D. Collin, A finite element analysis modeling tool for solid oxide fuel cell development: coupled electrochemistry, thermal and flow analysis in MARC, J. Power Sources 130 (2004) 136–148.
[4] K.P. Recknagle, R.E. Williford, L.A. Chick, D.R. Rector, M.A. Khaleel, Three-dimensional thermo-fluid electrochemical modeling of planar SOFC stacks, J. Power Sources 113 (2003) 109–114.
[5] H. Yakabe, T. Ogiwara, M. Hishinuma, I. Yasuda, 3D model calculation for planar SOFC, J. Power Sources 102 (2001) 144–154.
[6] R. Maric, S. Ohara, T. Fukui, H. Yoshida, M. Nishimura, T. Inagaki, K. Miura, Solid oxide fuel cells with doped lanthanum gallate electrolyte and $LaSrCoO_3$ cathode, and Ni-samaria-doped ceria cermet anode, J. Electrochem. Soc. 146 (1999) 2006–2010.

[7] J.W. Kim, A.V. Virkar, K.-Z. Fung, K. Mehta, S.C. Singhal, Polarization effects in intermediate temperature, anode-supported solid oxide fuel cells, J. Electrochem. Soc. 146 (1999) 69–78.
[8] A.V. Virkar, J. Chen, C.W. Tanner, J.W. Kim, The role of electrode microstructure on activation and concentration polarizations in solid oxide fuel cells, Solid State Ionics 131 (2000) 189–198.
[9] K. Huang, J.H. Wan, J.B. Goodenough, Increasing power density of LSGM-based solid oxide fuel cells using new anode materials, J. Electrochem. Soc. 148 (2001) A788–A794.
[10] H. Yakabe, M. Hishinuma, M. Uratani, Y. Matsuzaki, I. Yasuda, Evaluation and modeling of performance of anode-supported solid oxide fuel cell, J. Power Sources 86 (2000) 423–431.
[11] P. Aguiar, C.S. Adjiman, N.P. Brandon, Anode-supported intermediate temperature direct internal reforming solid oxide fuel cell. I. Model-based steady-state performance, J. Power Sources 138 (2004) 120–136.
[12] J.R. Ferguson, J.M. Fiard, R. Herbin, Three-dimensional numerical simulation for various geometries of solid oxide fuel cells, J. Power Sources 58 (1996) 109–122.
[13] S.H. Chan, K.A. Khor, Z.T. Xia, A complete polarization model of a solid oxide fuel cell and its sensitivity to the change of cell component thickness, J. Power Sources 93 (2001) 130–140.
[14] H. Zhu, R.J. Kee, A general mathematical model for analyzing the performance of fuel-cell membrane-electrode assemblies, J. Power Sources 117 (2003) 61–74.
[15] C.W. Tanner, K.Z. Fung, A.V. Virkar, Effect of porous composite electrode structure on solid oxide fuel cell performance. I. Theoretical analysis, J. Electrochem. Soc. 144 (1997) 21–30.
[16] W. Lehnert, J. Meusinger, F. Thom, Modeling of gas transport phenomena in SOFC anodes, J. Power Sources 87 (2000) 57–63.
[17] J. Fleig, Solid oxide fuel cell cathodes: polarization mechanisms and modeling of the electrochemical performance, Annu. Rev. Mater. Res. 33 (2003) 361–382.
[18] S. Sunde, Simulations of composite electrodes in fuel cells, J. Electroceram. 5 (2000) 153–182.
[19] M.M. Hussain, X. Li, I. Dincer, Multi-component mathematical model of solid oxide fuel cell anode, Int. J. Energy Res. 29 (2005) 1083–1101.
[20] R.E. Williford, L.A. Chick, Surface diffusion and concentration polarization on oxide-supported metal electrocatalyst particles, Surf. Sci. 547 (2003) 421–437.
[21] P. Costamagna, P. Costa, V. Antonucci, Micro-modeling of solid oxide fuel cell electrodes, Electrochim. Acta 43 (1998) 375–394.
[22] J. Newman, K.E. Thomas-Alyea, Electrochemical Systems, 3rd ed., Wiley, New Jersey, 2004.
[23] J. Deseure, Y. Bultel, L. Dessemond, E. Siebert, Theoretical optimization of a SOFC composite cathode, Electrochim. Acta 50 (2005) 2037–2046.
[24] W.A. Rogers, R.S. Gemmen, C. Johnson, M. Prinkey, M. Shahnam, Validation and application of a CFD-based model for solid oxide fuel cells and stacks, Fuel Cell Sci. Eng. Technol. ASME (2003) 517–520.
[25] M. Iwata, T. Hikosaka, M. Morita, T. Iwanari, K. Ito, K. Onda, Y. Esaki, Y. Sakaki, S. Nagata, Performance analysis of planar-type unit SOFC considering current and temperature distributions, Solid State Ionics 132 (2000) 297–308.
[26] R. Suwanwarangkul, E. Croiset, M.W. Fowler, P.L. Douglas, E. Entchev, M.A. Douglas, Performance comparison of Fick's, dusty-gas and Stefan-Maxwell models to predict the concentration overpotential of a SOFC anode, J. Power Sources 122 (2003) 9–18.
[27] M. Brown, S. Primdahl, M. Mogensen, Structure/performance relations for Ni/yttria-stablized zirconia anodes for solid oxide fuel cells, J. Electrochem. Soc. 147 (2000) 475–485.
[28] S.H. Chan, Z.T. Xia, Anode micro model of solid oxide fuel cell, J. Electrochem. Soc. 148 (2001) A388–A394.
[29] X.J. Chen, S.H. Chan, K.A. Khor, Simulation of a composite cathode in solid oxide fuel cells, Electrochim. Acta 49 (2004) 1851–1861.
[30] N.Q. Minh, T. Takahashi, Science and Technology of Ceramic Fuel Cells, Elsevier Science B.V., Amsterdam, The Netherlands, 1995.
[31] J.K. Rajesh, S.K. Gupta, G.P. Rangaiah, A.K. Ray, Multi-objective optimization of industrial hydrogen plants, Chem. Eng. Sci. 56 (2001) 999–1010.
[32] B.A. Haberman, J.B. Young, Three-dimensional simulation of chemically reacting gas flows in the porous support structure of an integrated-planar solid oxide fuel cell, Int. J. Heat Mass Transfer 47 (2004) 3617–3629.